Double Channel Neural Non Invasive Blood Pressure Prediction

Double Channel Neural Non Invasive Blood Pressure Prediction

heart and to other organs such as the kidneys, the brain and the eyes. Globally, hypertension kills roughly 8 million people per year [1][2].

Blood pressure is determined by the set of forces acting on the wall of the vessels: on one hand, the hydrostatic pressure exerted by the blood; on the other side, the resistance opposed by the vessel wall. The hydrostatic pressure depends on the strength and frequency with which the heart contracts by pumping the oxygenated blood, while the peripheral resistances depend on the extent of the blood flow, the elasticity and the diameter of the vessel wall: the smaller the vessel diameter, the higher the pressure inside them [3]. The complex physiological regulation system involves the autonomic nervous system (the part of the central nervous system responsible for controlling involuntary actions), some hormones and neuromodulators produced by the adrenal gland and the kidney that regulates the volume (total volume of blood) [4]. When one of these regulating elements is not able to respond appropriately to blood pressure variations, arterial hypertension may occur. The measurement of ABP consists of two quantities: the systole (SBP), determined by the peak pressure that is observed following the contraction of the left ventricle and the diastolic pressure (DBP), calculated during the relaxation phase. Due to ageing, diastolic blood pressure tends to decrease, while, at the same time, SBP increases; therefore, it is desirable to prevent the onset of the disease and report values out of the norm to ensure non-reversible damage. American Heart Association (AHA) classifies hypertension into four different stages, which characterize the individual's health status in relation to blood pressure values [5]. This is a great way to easily identify the severity level and find the most appropriate cure in a timely manner. Due to the importance of prevention, and to avoid the degeneration of hypertension, it is necessary to constantly keep both the pressure values under control [6].

Currently, there are two methodologies for ABP measurement. On one hand, an invasive method, based on an intra-arterial blood pressure (IBP) technique, which represents a direct measurement by inserting a cannula needle in a suitable artery. This method is employed in the Intensive Care Unit (ICU) and in the operating theatre and shows continuous patient monitoring of the arterial blood pressure together with its waveform visualization on a display. Unfortunately, this procedure may lead to pains and infections [7]. On the other hand, a non-invasive indirect method based on Korotkoff sounds. The most common device for indirect measurement is the sphygmomanometer, which returns the systolic and diastolic pressure values through the compression and decompression of a cuff, positioned around the patient's arm [8]; however, this procedure may lead to the misclassification of large numbers of patients because the model has inaccuracies. The non-invasive method proposed in this paper is based on the use of artificial neural networks (ANNs), which have been recently applied to medical problems, particularly in the fields of radiology, urology and cardiology. An ANN is a distributed network capable of identifying relationships in input data that are not easily evident with current common analytical techniques; in this sense, artificial neural networks can predict the relationships that exist between inputs and outputs [9]. In cardiology, artificial neural networks have been successfully applied to the diagnosis and treatment of coronary artery disease and myocardial infarction, in electrocardiographic interpretation and in arrhythmia detection and in image analysis in cardiac radiography [10]. Another application, related to blood, is a non-invasive practice for

determining hemoglobin concentration [11]. The trained model can be embedded in wearable devices, such as the ECG Watch [12] and the VITAL-ECG [13][14][15], for providing an anytime, everywhere, unobtrusive blood pressure measurement feature. In the proposed work, the neural network output error (NNOE) model, a recurrent neural network, has been implemented. NNOE is able to learn the physiological relation that exists between the inputs, the electrocardiographic (ECG) and the photoplethysmographic (PLETH/PPG) signals, and the output (the ABP value) [16]. The former represents the electrical signals in the heart, which are a consequence of cardiac muscle depolarization followed by repolarization during each cardiac cycle (heartbeat) [17]; PPG detects blood volume changes in the microvascular bed of tissue, in an optical way [18]. The rest of the paper is organized as follows: Sec. 2 carries out an analysis about the methodology for ABP estimation: the dataset used for the experiments is presented, the data pre-processing is detailed and the neural network architecture is accurately explained together with the chosen evaluation metrics. Sec. 3 details the experimental results, followed by the conclusions in Sec. 4.

2 Methodology

Fig. 1 shows the proposed framework, which is made of four main processing units:

1. Dataset description: data are extracted from MIMIC Database [19], in particular ECG, PPG are chosen as input and the IBP as target.
2. Data pre-processing: all signals are filtered with a moving mean; ECG is also filtered with a high-pass filter to remove disturbances that characterize the signal.
3. Neural Network: NNOE Neural Network Output Error [20], a recurrent neural network used to predict the values of IBP, both systolic and diastolic blood pressure values.
4. Metrics: SSE (sum-squared error) for MLP training and MAE (mean absolute error) to evaluate the quality of the forecasting.

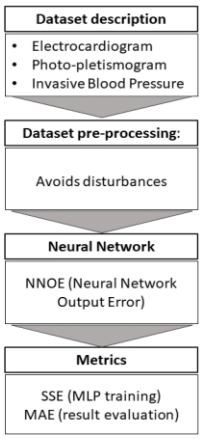

Fig. 1. Methodology of the proposed work

2.1 Dataset description

The goal of the work is to obtain a neural network trained in a way that, given the ECG and PPG inputs, returns a sufficiently accurate estimation of the ABP signal. Subsequently, the systolic and diastolic pressure is extracted from the peaks (SBP) and the valleys (DBP) of the ABP predicted signal.

The MIMIC (Multi-parameter Intelligent Monitoring for Intensive Care) Database is a collection of physiological signals from about 100 different patients, registered in the Intensive Care Units of medicine, surgery and cardiology of Boston's Beth Israel Hospital [19][21]. The recordings include continuous signals and periodic measurements extracted from the patient monitors and clinical data obtained from the records of each patient. The length of the data can vary from 20 to 40 hours, and the recordings from the patient monitors are divided into files of 10 minutes, which can be concatenated to obtain a single continuous signal. Fig. 2 shows the extracted signals from the MIMIC Database of a single patient (ECG, PPG and IBP). ECG and PPG represent the input signals, while IBP is the output. In this study, twenty-nine patients are considered. The results are analyzed comparing three different neural network configurations:

- ECG signal as input;
- PPG signal as input;
- ECG / PPG synchronized as an input (double channel).

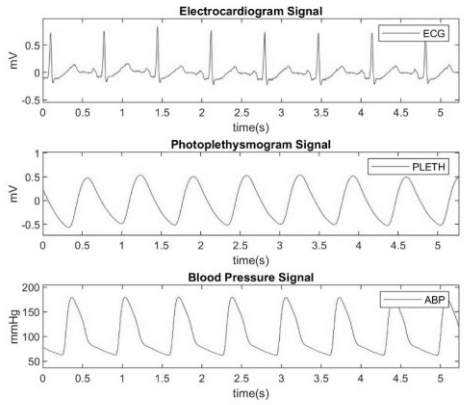

Fig. 2. Input signals (ECG and PPG) and output signal (IBP)

2.2 Data pre-processing

The ECG signal can mainly contain three types of noise:

- *Baseline wander*: low frequency noise around 0.5-0.6 Hz, which results in an oscillation around the baseline; it may be due to the use of incorrect electrodes (electrode-skin impedance), patient movements or breathing.

- *Power line interference*: around 50-60 Hz due to the electrical network; it can be removed using a notch filter with a cutoff frequency of 50-60 Hz.
- *Electromyography disturbance:* a high frequency noise, above 100 Hz, removed using a low pass filter having an appropriate cutoff frequency.

By analyzing the signals in the database, a high-pass filter is applied to the ECG signal to remove the *baseline wander*. Fig. 3 shows the signal improvement after the disturbance removal.

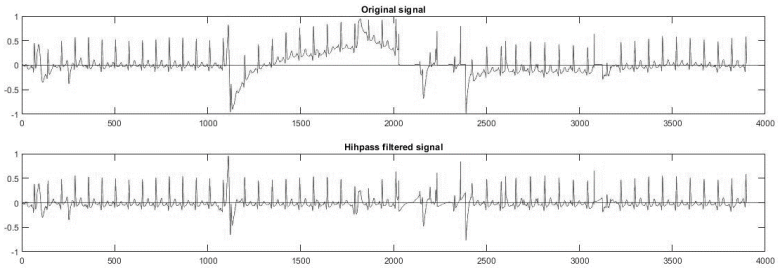

Fig. 3. Baseline wander removal from ECG signal

In addition, a moving mean filter is applied for removing the remaining noise in the three signals (ECG, PPG and ABP). The filter, with a window of 3 samples, represents the simplest form of a low-pass filter.

2.3 Neural Network Architecture – NNOE

There are basically two approaches to forecasting, which depend on the application [20]: the former uses the actual and previous values of the output in the regression vector (e.g. NARX and NARMAX), the latter uses only the previous predictions in the regression vector (e.g. NNOE). Obviously only the second case can be considered for ABP estimation, because the actual blood pressure information is not available.
The goal of the neural network output error (NNOE) is to implement a generic model structure for the identification of nonlinear dynamic systems in a stochastic environment. The basic structure of the neural network is a multilayer perceptron (MLP, [22]), which has the ability to model very complex continuous functional relationships.

Fig. 4 shows the workflow of the dynamical system identification.

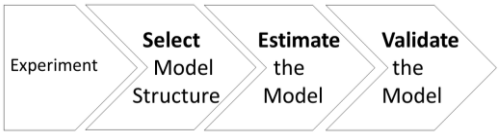

Fig. 4. Dynamical system identification

The experimental phase consists of the dataset collection, called Z^N, which describes the entire system with a sampling frequency:

$$Z^N = \{[u(t), y(t)|_{t=1,\dots,N}]\} \tag{1}$$

$u(t)$ and $y(t)$ represent the control signal and the measured output signal, respectively, where t specifies sampling instant.

For the selection of the model structure, a number of regressors is chosen based on the idea of a linear system identification, determining the network architecture optimization with the given regressors as inputs. For NNOE, the shape of the regression vector is given by:

$$\varphi(t) = [\hat{y}(t-1|\theta) \dots \hat{y}(t-n|\theta) \;\; u(t-d) \dots u(t-d-m)]^T \tag{2}$$

where θ is a vector containing the weights, n is the y-predicted lag, m is the input lag and d the delay to obtain the prediction. The vector of prediction is given by:

$$\hat{y}(t|\theta) = g(\varphi(t), \theta) \tag{3}$$

where g is the function realized by the artificial neural network.
The most common method of validation is the investigation of the residuals (prediction errors) by cross-validation on a test set.
NNOE has a predictor with a feedback through the choice of regressors, which in the neural network terminology means that the networks become recurrent: future network inputs will depend on present and past network outputs (see Fig. 5).

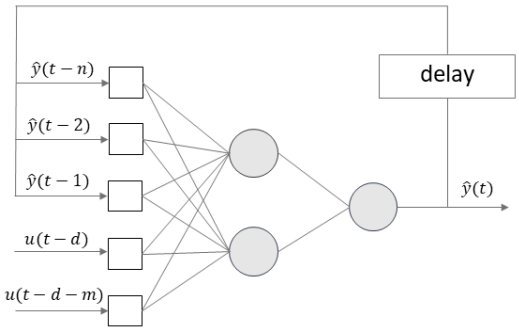

Fig. 5. Structure of NNOE model

2.4 Metrics

Two metrics are considered in this paper: the Sum of Squares Error (SSE) for the MLP training and the Mean Absolute Error (MAE) for the evaluation of the results. Both metrics express how much the network prediction is similar to the desired output (target).

The SSE metric quantifies how a dataset varies around a central number (like the mean). Generally, a lower residual sum of squares indicates that the regression model can better explain the data while a higher residual sum of squares indicates that the model poorly explains the data [23][24] .

$$SSE = \sum_i^n (y_i - \tilde{y}_i)^2 \tag{4}$$

MAE, instead, measures the average magnitude of the errors in a set of predictions, without considering their direction. It represents the average over the test sample of the absolute differences between prediction and actual observation where all individual differences have equal weight [25].

$$MAE = \frac{1}{n}\sum_i^n |y_i - \tilde{y}_i| \tag{5}$$

3 Results

In the following, three NNOE configurations have been compared with regard to the inputs; as shown in Fig. 6, the first one uses only ECG, the second one only PPG, while the latter both ECG and PPG as inputs.

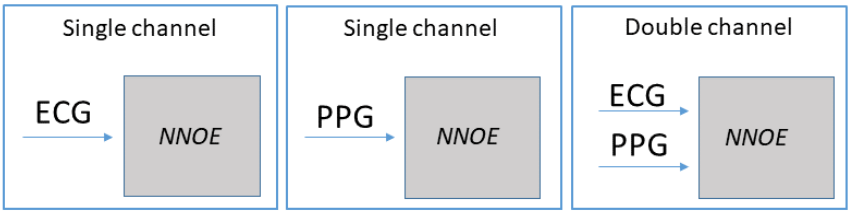

Fig. 6. NNOE input configurations. Single channel: ECG (left) or PPG (center); double channel: ECG and PPG (right).

The network optimal architecture is determined using a *trial-and-error* approach, where different numbers of hidden neurons and regressors were tested w.r.t. MAE. At the end, the chosen neural architecture consists of a multilayer perceptron (MLP) with fifty neurons and three regressors.

Fig. 7 and Fig. 8 show the MAE for SBP and DBP, respectively; for each patient (x axis) the MAEs of the three input configurations are grouped:

- the blue bar represents the network error with the electrocardiogram signal as input;
- the orange bar gives the performances with photoplethysmogram as input signal;
- the yellow bar shows the network MAE with the double channel (ECG and PPG).

To evaluate each input configuration quality, the MAEs have been averaged for all patients (excluding the outliers) as shown in Table 1: the double channel configuration has the best performance, with an average value of 2.42 and 3.17 for SBP and DBP, respectively.

Table 1. Systolic and diastolic blood pressure MAE (in mmHg) for the three different inputs.

Inputs	MAE (SBP)	MAE (DBP)
PPG	3.03	5.72
ECG	3.94	5.49
ECG/PPG	**2.42**	**3.17**

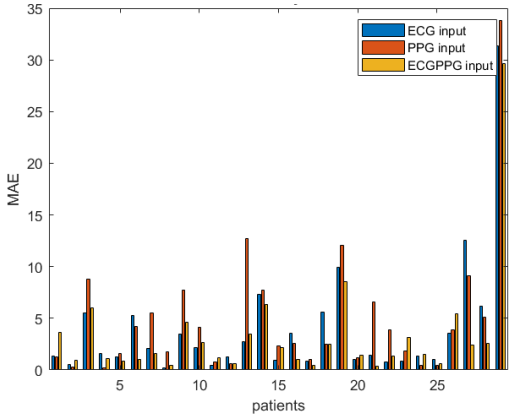

Fig. 7. Mean absolute error for SBP for every patient.

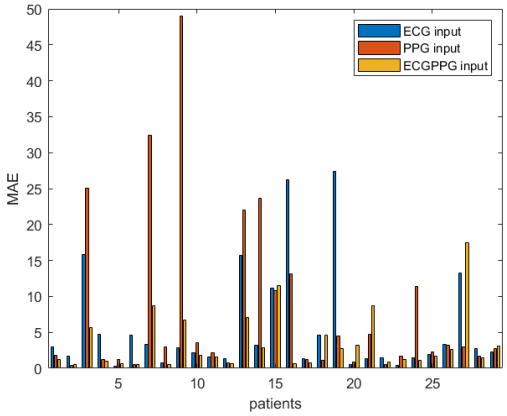

Fig. 8. Mean absolute error for DBP for every patient.

Because the analysis based only on the MAE metric is not sufficient to assess the quality of the proposed method, a deeper comparison between the desired target (IBP) and the NNOE predicted signal is performed. Fig. 9 shows the target-output signals plot for each input configuration for patient 2 (which has the lowest MAEs): the blue solid line represents the desired output (target) while the red dashed line the prediction signals. As can be seen, the double channel (ECG/PPG) is the best performing one.

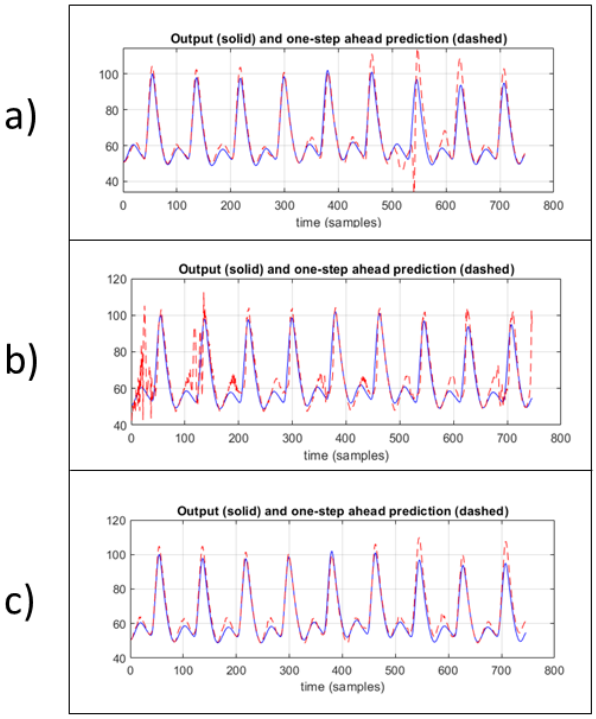

Fig. 9. Output vs. target signals for each input configuration: ECG (a), PPG (b), ECG/PPG (c).

3.1 Discussion

Some considerations can be drawn just by considering one patient (here patient 2). The Spearman's rank correlation coefficient measures the non linear correlation between two variables. For ECG and ABP, it is equal to 0.17, while for PPG and ABP, it is equal to 0.37. Hence, PPG is more correlated to ABP than ECG. Furthermore, the test SSE for the NNOE model of the relationship between PPG and ABP is equal to 3.19×10^4, and for the relationship between ECG and ABP is equal to 3.42×10^4. All these estimates prove PPG is better related to ABP than ECG. So, why does ECG yield a better estimation of ABP? To answer this question, it must be considered that the goal of the algorithm is the accurate evaluation of SBP and DBP. As seen before, the most difficult evaluation is SBP, which depends on the slope of the signal, i.e. its derivative. This first order rate is proportional to the latency time of the phenomenon. ECG is immediately related to ABP, because the pressure depends on the heartbeat. On the contrary, PPG depends on the level of oxygen in blood, which in turn depends on the global cardio-circulatory apparatus: hence it requires a longer time to follow the blood pressure rate of change. These considerations are also confirmed in Fig. 2, which shows that the PPG signal has a slower rate of change in the peaks than the other two signals. It can be deduced that the PPG inertia prevents from the accurate synchronous detection of the

pressure peaks. Concluding, despite the fact that PPG better represents the ABP signal, ECG better estimates the ABP peaks. In the case of two channels, the pros of both ECG and PPG yield the best result.

4 Conclusion

In this paper, a non invasive blood pressure estimation technique is presented. To determine the best input among a single (ECG or PPG) and a double channel (synchronized ECG and PPG) configurations, a comparative analysis is carried out. Because the goal is the ABP forecasting, the NNOE method is used, which is a recurrent neural network, based on MLP, employing only the previous predictions in the regression vector. The algorithm is tested on twenty-nine subjects by always using the IBP as target signal for training. From each predicted signal, peaks and valleys have been extracted to compute the corresponding SBP and DBP values; then, they are compared with ABP ones in terms of MAE as required by ANSI/AAMI/ ISO 81060- 2:2013 regulation for non invasive ABP techniques. The double channel configuration yields the best results w.r.t. mean absolute error, which results to be, on average, 2.42 mmHg and 3.17 mmHg for SBP and DBP, respectively; in this sense, this configuration is compliant with the legislation because the estimated values are within +/- 5 mmHg w.r.t. real invasive measurements. Among the single input configurations, ECG performs better than PPG w.r.t. MAE; on the contrary, the Spearman's coefficients between the ABP and the two inputs suggests an opposite relationship. This behavior is explained by the human biology and the SBP latency time: ECG is immediately related to ABP by means of the heartbeat, while PPG is related to the global cardio-circulatory apparatus, which requires a longer time to follow the blood pressure rate of change. In this sense, PPG inertia prevents from the accurate synchronous detection of the pressure peaks.

The proposed technique can be embedded in wearable portable devices to perform continuous monitoring of vital parameters to prevent the onset of cardiovascular diseases, such us hypertension; indeed, the neural approach can be exploited to fight CVDs and reduce the amount of people, who die for such pathologies.

Future work will deal with an extensive comparison with deep neural networks, e.g. convolution neural networks. It will be also further analyzed the use of the recurrent neural networks, already used in this experiment [26]. Furthermore, a deeper study of specificity and sensitivity w.r.t. the single patient will be conducted; an unsupervised patient clustering will be exploited for tuning supervised neural networks specific for each cluster, such an approach could be useful to improve the generalization capability of the proposed approach.

References

[1] C. Kumar, V. Sagar, M. Kumar, and K. Kiran, "Awareness about hypertension and its modifiable risk factors among adult population in a rural area of Ranchi district of Jharkhand, India," *Int. J. Community Med. Public Heal.*, vol. 3, no. 5, pp. 1069–1073,

Feb. 2016, doi: 10.18203/2394-6040.ijcmph20161359.

[2] A. A. Leung *et al.*, "Hypertension Canada's 2017 Guidelines for Diagnosis, Risk Assessment, Prevention, and Treatment of Hypertension in Adults," *Can. J. Cardiol.*, vol. 33, no. 5, pp. 557–576, May 2017, doi: 10.1016/j.cjca.2017.03.005.

[3] J. Järhult and S. Mellander, "Autoregulation of Capillary Hydrostatic Pressure in Skeletal Muscle during Regional Arterial Hypo- and Hypertension," *Acta Physiol. Scand.*, vol. 91, no. 1, pp. 32–41, May 1974, doi: 10.1111/j.1748-1716.1974.tb05654.x.

[4] P. A. James *et al.*, "2014 Evidence-based guideline for the management of high blood pressure in adults: Report from the panel members appointed to the Eighth Joint National Committee (JNC 8)," *JAMA - Journal of the American Medical Association*, vol. 311, no. 5. American Medical Association, pp. 507–520, 2014, doi: 10.1001/jama.2013.284427.

[5] "Understanding Blood Pressure Readings | American Heart Association." [Online]. Available: https://www.heart.org/en/health-topics/high-blood-pressure/understanding-blood-pressure-readings. [Accessed: 11-May-2020].

[6] C. Torlasco *et al.*, "[BP.03.03] CARDIOVASCULAR RISK AND HYPERTENSION CONTROL IN ITALY. DATA FROM THE 2015 WORLD HYPERTENSION DAY," *J. Hypertens.*, vol. 35, pp. e176–e177, Sep. 2017, doi: 10.1097/01.hjh.0000523480.78727.21.

[7] C. Pellaton *et al.*, "Accuracy testing of a new optical device for noninvasive estimation of systolic and diastolic blood pressure compared to intra-arterial measurements," *Blood Press. Monit.*, vol. 25, no. 2, pp. 105–109, 2020, doi: 10.1097/MBP.0000000000000421.

[8] T. G. Pickering *et al.*, "Recommendations for blood pressure measurement in humans and experimental animals: Part 1: Blood pressure measurement in humans - A statement for professionals from the Subcommittee of Professional and Public Education of the American Heart Association Council on high blood pressure research," *Circulation*, vol. 111, no. 5. Circulation, pp. 697–716, 08-Feb-2005, doi: 10.1161/01.CIR.0000154900.76284.F6.

[9] F. Menolascina *et al.*, "Developing optimal input design strategies in cancer systems biology with applications to microfluidic device engineering," *BMC Bioinformatics*, vol. 10, no. SUPPL. 12, p. S4, Oct. 2009, doi: 10.1186/1471-2105-10-S12-S4.

[10] D. Itchhaporia, P. B. Snow, R. J. Almassy, and W. J. Oetgen, "Artificial neural networks: Current status in cardiovascular medicine," *J. Am. Coll. Cardiol.*, vol. 28, no. 2, pp. 515–521, Aug. 1996, doi: 10.1016/0735-1097(96)00174-x.

[11] V. Bevilacqua *et al.*, "A novel approach to evaluate blood parameters using computer vision techniques," in *2016 IEEE International Symposium on Medical Measurements and Applications, MeMeA 2016 - Proceedings*, 2016, doi: 10.1109/MeMeA.2016.7533760.

[12] V. Randazzo, J. Ferretti, and E. Pasero, "ECG WATCH: A real time wireless wearable ECG," in *Medical Measurements and Applications, MeMeA 2019 - Symposium Proceedings*, 2019, doi: 10.1109/MeMeA.2019.8802210.

[13] Randazzo, Ferretti, and Pasero, "A Wearable Smart Device to Monitor Multiple Vital Parameters—VITAL ECG," *Electronics*, vol. 9, no. 2, p. 300, Feb. 2020, doi: 10.3390/electronics9020300.

[14] V. Randazzo, E. Pasero, and S. Navaretti, “VITAL-ECG: A portable wearable hospital,” in *2018 IEEE Sensors Applications Symposium, SAS 2018 - Proceedings*, 2018, vol. 2018-January, pp. 1–6, doi: 10.1109/SAS.2018.8336776.

[15] A. Paviglianiti and E. Pasero, “VITAL-ECG: a de-bias algorithm embedded in a gender-immune device,” in *2020 IEEE International Workshop on Metrology for Industry 4.0 & IoT*, 2020, pp. 314–318, doi: 10.1109/MetroInd4.0IoT48571.2020.9138291.

[16] A. Paviglianiti, V. Randazzo, E. Pasero, and A. Vallan, “Noninvasive Arterial Blood Pressure Estimation using ABPNet and VITAL-ECG,” in *I2MTC 2020 - International Instrumentation and Measurement Technology Conference, Proceedings*, 2020, doi: 10.1109/I2MTC43012.2020.9129361.

[17] C. P. Chua and C. Heneghan, “Continuous blood pressure monitoring using ECG and finger photoplethysmogram,” in *Annual International Conference of the IEEE Engineering in Medicine and Biology - Proceedings*, 2006, pp. 5117–5120, doi: 10.1109/IEMBS.2006.259612.

[18] E. C. P. Chua, S. J. Redmond, G. McDarby, and C. Heneghan, “Towards using photo-plethysmogram amplitude to measure blood pressure during sleep,” in *Annals of Biomedical Engineering*, 2010, vol. 38, no. 3, pp. 945–954, doi: 10.1007/s10439-009-9882-z.

[19] G. B. Moody and R. G. Mark, “A database to support development and evaluation of intelligent intensive care monitoring,” *Comput. Cardiol.*, vol. 0, no. 0, pp. 657–660, 1996, doi: 10.1109/cic.1996.542622.

[20] M. Nørgaard, *Neural networks for modelling and control of dynamic systems : a practitioner s handbook*. Springer, 2000.

[21] A. L. Goldberger *et al.*, “PhysioBank, PhysioToolkit, and PhysioNet: components of a new research resource for complex physiologic signals.,” *Circulation*, vol. 101, no. 23, 2000, doi: 10.1161/01.cir.101.23.e215.

[22] S. Haykin, *Neural Networks: A Comprehensive Foundation (3rd Edition)*, vol. 13, no. 4. Prentice-Hall, Inc. Upper Saddle River, NJ, USA ©2007, 1999.

[23] D. F. Specht, “Brief Papers A General Regression Neural Network.”

[24] J. O. Rawlings, S. G. Pantula, and D. A. D. Springer, “Applied Regression Analysis: A Research Tool, Second Edition.”

[25] C. Willmott and K. Matsuura, “Advantages of the mean absolute error (MAE) over the root mean square error (RMSE) in assessing average model performance,” *Clim. Res.*, vol. 30, no. 1, pp. 79–82, Dec. 2005, doi: 10.3354/cr030079.

[26] A. Paviglianiti, V. Randazzo, G. Cirrincione, and E. Pasero, “Neural Recurrent Approches to Noninvasive Blood Pressure Estimation,” in *2020 International Joint Conference on Neural Networks (IJCNN)*, 2020.